UCLA
COMPUTATIONAL AND APPLIED MATHEMATICS

Non-Oscillatory Boundary Treatment for Staggered Central Schemes

Doron Levy
Eitan Tadmor

January 1998

CAM Report 98-1

Department of Mathematics
University of California, Los Angeles
Los Angeles, CA. 90095-1555

003

Non-Oscillatory Boundary Treatment for Staggered Central Schemes

Doron Levy[†‡] Eitan Tadmor[†§]

September 2, 1997

Abstract

We are concerned with numerical schemes for solving nonlinear hyperbolic conservation laws subject to prescribed initial values and to Dirichlet boundary conditions in inflow boundaries. We focus on a family of high-resolution, non-oscillatory, staggered *central* schemes for approximating solutions of such nonlinear problems. For these schemes we present a non-oscillatory staggered boundary treatment which is based on a natural extension of the interior central scheme up to the boundary. The desired non-oscillatory properties of this treatment are clearly seen in the numerical examples we present.

Contents

1 Introduction

In recent years, central schemes for approximating solutions of hyperbolic conservation laws, received a lot of attention. A family of high-resolution, non-oscillatory, *central* schemes, was developed to handle such problems. Compared with the 'classical' *upwind* schemes, these *central* schemes were shown to be both simple and stable for a large variety of problems ranging from one-dimensional scalar problems to multi-dimensional systems of conservation laws. They were successfully implemented for a variety of other related problems, such as, e.g., the incompressible Euler equations [13], the magneto-hydrodynamics equations [23], hyperbolic systems with relaxation source terms [3], non-linear optics [19] and slow moving shocks [9].

Yet, in terms of both theoretical and applicative points of view, some questions regarding these schemes remained uninvestigated. Here we address one of these important issues – namely, the question of how to impose *non-oscillatory Dirichlet boundary conditions*.

The family of high-order *central* schemes we deal with, can be viewed as a direct extension to the first-order, Lax-Friedrichs (LxF) scheme [4], which on one hand is robust and stable, but on the other

[†]School of Mathematical Sciences, Tel-Aviv University, Tel-Aviv 69978 Israel

[‡]Département de Mathématiques, Ecole Normale Supérieure, 45 rue d'Ulm, 75230 Paris Cedex 05 France; Email: dlevy@dmi.ens.fr

[§]Department of Mathematics, UCLA, Los-Angeles CA 90095; Email: tadmor@math.ucla.edu

hand suffers from excessive dissipation. To address this problematic property of the LxF scheme, a Godunov-like second-order central scheme was developed by Nessyahu and Tadmor (NT) in [16] (see also [21]). It was extended to higher-order of accuracy as well as for more space dimensions (consult [1], [2] and [8] for the two-dimensional case, and [20], [15] and [12] for the third-order schemes).

The NT scheme is based on reconstructing, in each time step, a piecewise-polynomial interpolant from the cell-averages computed in the previous time step. This interpolant is then (exactly) evolved in time, and finally, it is projected on its staggered averages, resulting with the staggered cell-averages at the next time-step. The one- and two-dimensional second-order schemes, are based on a piecewise-linear MUSCL-type reconstruction, whereas the third-order schemes are based on the non-oscillatory piecewise-parabolic reconstruction [14].

Like *upwind* schemes, the reconstructed piecewise-polynomials used by the central schemes, also make use of non-linear limiters which guarantee the overall non-oscillatory nature of the approximate solution. But unlike the upwind schemes, central schemes avoid the intricate and time consuming Riemann solvers; this advantage is particularly important in the multi-dimensional setup – where no such Riemann solvers exist.

To this family of central schemes, we present a natural non-oscillatory boundary treatment. Our boundary scheme is constructed using the exact basic principles used for the derivation of the aforementioned family of central schemes. Following this construction we show how to complement the scheme with Dirichlet boundary conditions at inflow boundaries without creating spurious oscillations. Most importantly, this boundary scheme is problem independent and it enjoys the overall simplicity and advantages of the central interior scheme.

The paper is organized as follows:

In §2 we briefly overview the construction of the family of central schemes, focusing on the one- and two-dimensional second-order scheme.

In §3 we present a natural way to deal with boundary conditions. We start by presenting our general ideas in the framework of the one-dimensional scalar hyperbolic conservation law, and then extend this boundary treatment to systems and to more space dimensions. We emphasize that a non-oscillatory boundary treatment is indeed an intricate task, and demonstrate the oscillations that develop with a naive boundary treatment.

We end in §4 by presenting a couple of examples in which the above boundary treatment was implemented. These examples, clearly show that our treatment does not produce any spurious oscillations at the boundary, and by that it clearly enjoys the robust nature of the entire interior schemes.

Acknowledgment: Research was supported by ONR Grant #N00014-91-J-1076, NSF Grant #DMS94-04942 and by the Sackler Institute for Scientific Computations in TAU. Part of this work was carried out at the Mathematics department of UCLA. D.L. would also like to thank the UCLA Mathematics department for its warm hospitality.

2 A Short Guide to Central Schemes

In this section we briefly overview the construction of the family of high-order, non-oscillatory, central schemes for approximating solutions of hyperbolic conservation laws. We start by considering the one-dimensional hyperbolic system of conservation laws

$$u_t + f(u)_x = 0, \tag{2.1}$$

subject to the initial data, $u(x, t = 0) = u_0(x)$. To approximate solutions of (2.1), we introduce a mesh in the $x - t$ plane, the spatial grid-points are denoted by x_j. We denote by Δx and Δt, the spacing in the x and in the t variables respectively, and abbreviate by I_j the cell around x_j, i.e., $I_j := \{\xi \big| |\xi - x_j| \leq \frac{\Delta x}{2}\}$.

By $w_j \sim u(x_j)$, we denote the approximate solution at x_j, and define $\bar{w}_j$ as the average of w_j over the cell I_j. Here, we follow Nessyahu and Tadmor (NT) [16] in the reconstruction of the second-order, non-oscillatory central scheme. To approximate solutions of (2.1), we introduce a piecewise-linear

approximate solution at the discrete time levels, $t^n = n\Delta t$, based on linear functions $p_j(x,t^n)$ which are supported at the cells I_j (see Figure 1),

$$w(x,t)|_{t=t^n} = \sum_j p_j(x,t^n)\chi_j(x) := \sum_j \left[\bar{w}_j^n + w_j'\left(\frac{x-x_j}{\Delta x}\right)\right]\chi_j(x), \qquad \chi_j(x) := 1_{I_j}. \tag{2.2}$$

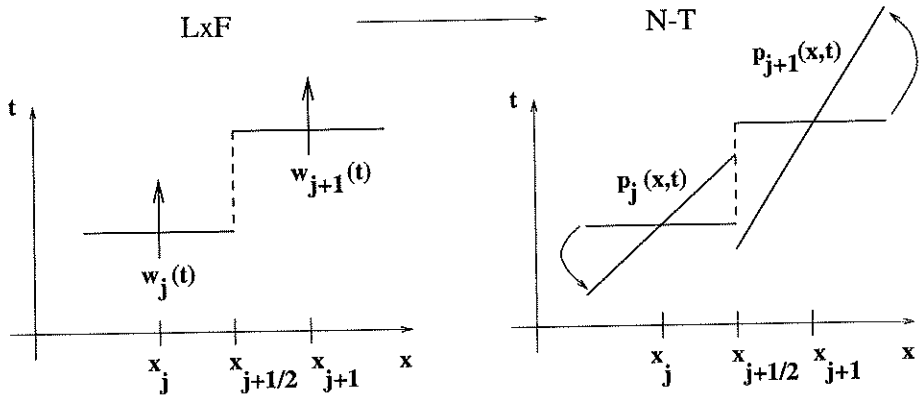

Figure 1: The second-order reconstruction

Second-order of accuracy is guaranteed if the discrete slopes approximate the corresponding derivatives, $w_j' \sim \Delta x \cdot \partial_x w(x_j,t^n) + O(\Delta x)^2$. Such a non-oscillatory approximation of the derivatives is possible, e.g., by using built-in non-linear limiters of the form

$$w_j' = MM\{\theta(\bar{w}_{j+1}^n - \bar{w}_j^n), \frac{1}{2}(\bar{w}_{j+1}^n - \bar{w}_{j-1}^n), \theta(\bar{w}_j^n - \bar{w}_{j-1}^n)\}. \tag{2.3}$$

Here and below, $\theta \in (0,2)$ is a non-oscillatory limiter and MM denotes the Min-Mod function

$$MM\{x_1,x_2,...\} = \begin{cases} \min_i\{x_i\} & \text{if } x_i > 0, \forall i \\ \max_i\{x_i\} & \text{if } x_i < 0, \forall i \\ 0 & \text{otherwise.} \end{cases}$$

An *exact* evolution of w, based on integration of the conservation law over the staggered cell, $I_{j+\frac{1}{2}}$, then reads

$$\bar{w}_{j+\frac{1}{2}}^{n+1} = \frac{1}{\Delta x}\int_{I_{j+\frac{1}{2}}} w(x,t^n)dx - \frac{1}{\Delta x}\int_{\tau=t^n}^{t^{n+1}} \left[f(w(x_{j+1},\tau)) - f(w(x_j,\tau))\right]d\tau.$$

The first integral is the staggered cell-average at time t^n, $\bar{w}_{j+\frac{1}{2}}^n$, which can be computed directly from the above reconstruction. The time integrals of the flux are computed by the second-order accurate mid-point quadrature rule. Here, the Taylor expansion is being used to predict the required mid-values of w. The scheme can be therefore formulated in a predictor-corrector form: a *predictor step*

$$w_j^{n+1/2} = w_j^n - \frac{\lambda}{2}f_j', \qquad f_j' = f_u(w_j)w_j' =: A(w_j)w_j', \tag{2.4}$$

which is followed by the *corrector* step

$$\bar{w}_{j+\frac{1}{2}}^{n+1} = \frac{1}{2}(\bar{w}_j^n + \bar{w}_{j+1}^n) + \frac{1}{8}(w_j' - w_{j+1}') - \lambda\left[f(w_{j+1}^{n+1/2}) - f(w_j^{1/2})\right]. \tag{2.5}$$

To upgrade this scheme into a third-order accurate scheme one has to use (consult [15])

- A piecewise-parabolic reconstruction which replaces the piecewise-linear reconstruction.
- A more accurate quadrature rule for the flux integral which replaces the mid-point quadrature rule.

- A second-order accurate Taylor expansion to predict the mid-values which replaces the corresponding first-order expansion.

Following the same lines, one can derive a non-oscillatory, two-dimensional central scheme. Here we sketch the construction of the second-order two-dimensional scheme following [8] (see also [1]). For the two-dimensional third-order accurate scheme, we refer to [12].

We consider the two-dimensional hyperbolic system of conservation laws

$$u_t + f(u)_x + g(u)_y = 0. \tag{2.6}$$

To approximate a solution to (2.6), we start with a two-dimensional linear reconstruction

$$w(x,y,t^n) = \sum_{j,k} p_{j,k}(x,y)\chi_{j,k}(x,y), \quad p_{j,k}(x,y) = \bar{w}^n_{j,k} + w'_{j,k}\left(\frac{x-x_j}{\Delta x}\right) + w\backslash_{j,k}\left(\frac{y-y_k}{\Delta y}\right). \tag{2.7}$$

Here, the discrete slopes in the x and in the y direction approximate the corresponding derivatives, $w'_{j,k} \sim \Delta x \cdot w_x(x_j,y_k,t^n) + O(\Delta x)^2$, $w\backslash_{j,k} \sim \Delta y \cdot w_y(x_j,y_k,t^n) + O(\Delta y)^2$, and $\chi_{j,k}(x,y)$ is the characteristic function of the cell $I_{j,k} := \left\{(\xi,\eta)\middle| |\xi - x_j| \le \frac{\Delta x}{2}, |\eta - y_k| \le \frac{\Delta y}{2}\right\}$.

An exact evolution of this reconstruction, which is based on integration of the conservation law over the staggered volume, followed by a mid-point approximation to the integrals of the fluxes, can be formulated in a predictor-corrector form, with the *predictor step*

$$w^{n+\frac{1}{2}}_{j,k} = w^n_{j,k} - \frac{\lambda}{2} f'_{j,k} - \frac{\mu}{2} g\backslash_{j,k}, \tag{2.8}$$

and the *corrector step*

$$\begin{aligned} \bar{w}^{n+1}_{j+\frac{1}{2},k+\frac{1}{2}} &= < \frac{1}{4}(\bar{w}^n_{j,\cdot} + \bar{w}^n_{j+1,\cdot}) + \frac{1}{8}(w'_{j,\cdot} - w'_{j+1,\cdot}) - \lambda(f^{n+\frac{1}{2}}_{j+1,\cdot} - f^{n+\frac{1}{2}}_{j,\cdot}) >_{k+\frac{1}{2}} + \\ &+ < \frac{1}{4}(\bar{w}^n_{\cdot,k} + \bar{w}^n_{\cdot,k+1}) + \frac{1}{8}(w\backslash_{\cdot,k} - w\backslash_{\cdot,k+1}) - \mu(g^{n+\frac{1}{2}}_{\cdot,k+1} - g^{n+\frac{1}{2}}_{\cdot,k}) >_{j+\frac{1}{2}} . \end{aligned}$$

Here are below, $\lambda := \frac{\Delta t}{\Delta x}$ and $\mu := \frac{\Delta t}{\Delta y}$ denote the fixed mesh-ratios, and we used the staggered averaging notation

$$< w_{j,\cdot} >_{k+\frac{1}{2}} := \frac{1}{2}(w_{j,k} + w_{j,k+1}), \quad < w_{\cdot,k} >_{j+\frac{1}{2}} := \frac{1}{2}(w_{j,k} + w_{j+1,k}).$$

3 Numerical Treatment of Boundary Conditions

In this section we construct a non-oscillatory boundary scheme that augments the interior scheme we overviewed in §2. We start by constructing such a scheme for the one-dimensional case. We then extend this boundary scheme to two space dimensions.

3.1 The scalar One-Dimensional Setup

The *central* schemes we overviewed in §2 are based on a staggered grid. Consequently, the boundary scheme we present here, is composed from two steps, dictated by the two phases of the boundary cells. In one step of the scheme, we compute the cell-average on the boundary *half-cell*, whereas in the following step, this half cell-average is used to compute the average on a whole boundary cell (see Figure 2). This separation into two phases is only technical – the *arguments* used to construct the boundary scheme in one phase, are identical to those used at the second phase. We start with the first phase of this computation.

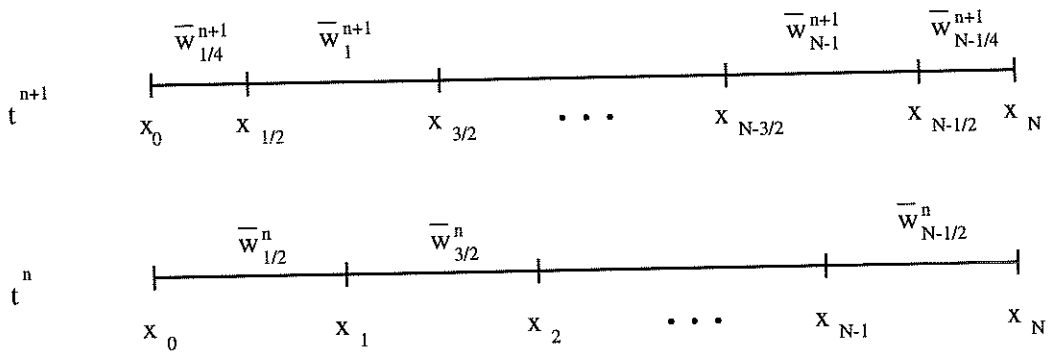

Figure 2: one dimensional stencil

Here, we assume that the cell averages, $\bar{w}^n_{1/2}, \bar{w}^n_{3/2} \cdots, \bar{w}^n_{N-1/2}$, are given at time $t = t^n$, and we wish to compute the cell averages, $\bar{w}^{n+1}_{1/4}$, $\bar{w}^{n+1}_{j\,(j=1,..,N-1)}$, $\bar{w}^{n+1}_{N-\frac{1}{4}}$, at the next time-step t^{n+1}. In the following we discuss the boundary treatment at the left boundary. An analogous treatment holds for the right boundary.

To follow the setup dictated by the differential level, we have to distinguish between two possible situations: the left boundary is either an *inflow* boundary, i.e., $f'(w^n_{1/2}) > 0$, or an *outflow* boundary, $f'(w^n_{1/2}) < 0$.

We start by assuming that the left boundary is an *inflow* boundary and hence data propagates into the interior of the domain. Consequently, the point-values at the boundary, w_0, must be prescribed. We now elaborate on the computation of the next, half-cell average, $\bar{w}^{n+1}_{1/4}$.

At such inflow boundary-cell, $I_{1/2}$, the reconstructed interpolant is given by (consult (2.2))

$$p_{1/2}(x, t^n) = \bar{w}^n_{1/2} + w'_{1/2}\left(\frac{x - x_{1/2}}{\Delta x}\right). \tag{3.1}$$

The cell-average, $\bar{w}^n_{1/2}$, was already computed at the previous time-step; how to reconstruct the discrete slope, $w'_{1/2}$, at the boundary cell, $I_{1/2}$? Here we are dealing with an inflow boundary and thus the point-value, w^n_0, is prescribed. Consequently, we may use the prescribed boundary point-values to uniquely determine the discrete slope, $w'_{1/2}$, as

$$w'_{1/2} = 2(\bar{w}^n_{1/2} - w^n_0). \tag{3.2}$$

This procedure, however, does not limit the discrete slope at the boundary cell, by using a limiting procedure which was used to prevent spurious oscillations at the interior cells, see (2.3). Consequently, the reconstruction (3.1) may develop spurious oscillations at the boundary, which will then propagate and contaminate also the interior of the domain.

In Figure 3 we demonstrated a typical situations in which spurious oscillations develop at the boundary. Here, we solved (2.1) with the initial data

$$u_0(x) = -5x^3, \quad x \in [-1, 1],$$

and the inflow boundary conditions, $u(-1, t) = 5$, $u(1, t) = -5$. On the boundary cells, we used a linear reconstruction whose slopes where determined according to (3.2).

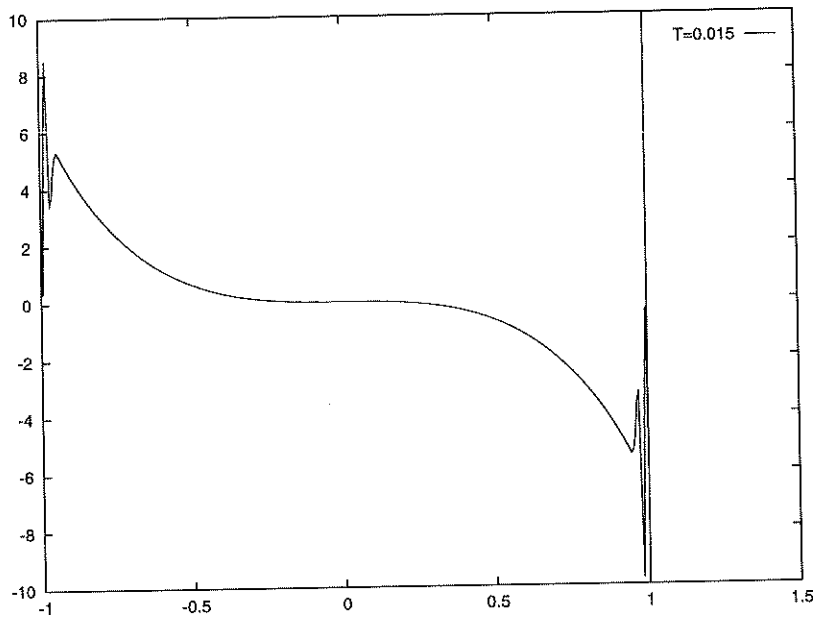

Figure 3: Oscillations at the boundaries with naive boundary treatment

In order to avoid such undesirable oscillations, we limit ourselves to a constant interpolant at such boundary cell, where $w'_{1/2} = 0$, i.e.

$$p_{1/2}(x, t^n) \equiv w_0^n. \tag{3.3}$$

Clearly, this is non-oscillatory; at the same time, this first-order boundary treatment will suffice for a second-order accurate interior scheme.

Since a constant solution remains constant in time, the predicted required value at $(x_{1/2}, t^{n+1/2})$, which is needed for the mid-point flux quadrature, is given by

$$w_{1/2}^{n+1/2} = p_{1/2}(x_{1/2}, t^n) = w_0^n. \tag{3.4}$$

We are now in a position to compute the cell-averages at the next time-step, t^{n+1}. The cell-averages at the interior cells, $\bar{w}_j^{n+1}$, $j = 1, \ldots, N-1$, can be now computed utilizing (3.3) and (3.4). In particular, the new cell-average, w_1^{n+1}, is now influenced by our boundary reconstruction which in this fashion, propagates intro the interior domain.

Finally, it remains to compute the cell-averages at the left boundary cell $\bar{w}_{1/4}^{n+1}$ (and, respectively, at the right boundary cell, $\bar{w}_{N-\frac{1}{4}}^{n+1}$). Since we are dealing with an inflow boundary, and hence, assume that the point-values are prescribed at that boundary, we have to assume that in particular, the point-value at the left corner, w_0^{n+1}, is also known at the next time step. As before, we define the cell average at the left boundary cell as the prescribed boundary value

$$\bar{w}_{1/4}^{n+1} := w_0^{n+1}.$$

We now turn to the case of an *outflow* left boundary. At such a boundary, data propagates from the interior of the domain up to the boundary and hence, all the required quantities are extrapolated from the interior of the domain up to the boundary. We elaborate on our arguments.

We first notice that the slope in any piecewise-linear "cell" is constant through the cell. In particular, $w'_0 = w'_{1/2}$. Utilizing a Taylor expansion, the predicted mid-value at the boundary equals

$$w_0^{n+1/2} = w_0^n - \frac{\lambda}{2} f'_0, \tag{3.5}$$

with

$$w_0^n = w_{1/2}^n - \frac{\Delta x}{2} w'_{1/2}, \qquad f'_0 = A(w_0^n) w'_0, \qquad w'_0 = w'_{1/2}.$$

Since in the outflow case, there is a contribution only from one side of the boundary, the boundary cell average at t^{n+1} is given by integration over the control volume $I_{1/4} \times [t^n, t^{n+1}]$, which leads to the *corrector step*

$$\bar{w}_{1/4}^{n+1} = \bar{w}_{1/2}^{n} - \frac{1}{4} w'_{1/2} - \lambda \left[f(w_{1/2}^{n+1/2}) - f(w_0^{n+1/2}) \right]. \tag{3.6}$$

This concludes phase I.

In the second phase of the staggering, we assume that the cell-averages, $\bar{w}_{1/4}, \bar{w}_j^{n+1}{}_{j=1,\ldots,N}, \bar{w}_{N-1/4}^{n+1}$, are given, and we compute the cell averages at the next time step, $\bar{w}_{1/2}^{n+2}, \bar{w}_{3/2}^{n+2}, \ldots, \bar{w}_{N-1/2}^{n+2}$. This is done by following the same arguments as in the first phase of the staggering. The type of reconstruction on the boundary depends on the type of the flow: constant reconstruction at an *inflow* boundary, and linear reconstruction at an *outflow* boundary (with the required quantities extrapolated from the interior of the domain).

The entire boundary treatment is summarized in the following:

Phase I (of the staggering): Determine the type of the flow at the left boundary.

- Inflow ($f'(w_{1/2}^n) > 0$):

  $p_{1/2}(x, t^n) \equiv w_0^n, \quad w'_{1/2} = 0$ — Piecewise-constant reconstruction on the boundary cell.

  $\bar{w}_j^{n+1} = \ldots \ {}_{(j=1,\ldots,N-1)}$ — The interior scheme.

  $\bar{w}_{1/4}^{n+1} = w_0^{n+1}$ — The cell-average at the boundary cell equals to the prescribed point-value at the boundary.

- Outflow ($f'(w_{1/2}^n) < 0$):

  $w'_{1/2} = \ldots$ — One-sided approximation.

  $w_0^n = w_{1/2}^n - \frac{\Delta x}{2} w'_{1/2}, \quad f'_0 = A(w_0^n) w'_{1/2}$

  $w_0^{n+1/2} = w_0^n - \frac{\lambda}{2} f'_0$

  $\bar{w}_{1/4}^{n+1} = \bar{w}_{1/2}^n - \frac{1}{4} w'_{1/2} - \lambda [f(w_{1/2}^{n+1/2}) - f(w_0^{n+1/2})]$ — The cell-average at the boundary cell.

Repeat analogously for the right boundary and then for the second phase of the staggering.

Note that the overall second-order accuracy of the scheme is retained when using such a first-order constant reconstruction at the boundary. Also, using the *exact* given boundary data, retains the desired local accuracy at the boundary.

3.2 Extensions to Systems

An analogous boundary treatment is also valid for systems. One is required to distinguish only on boundary cells, between the inflow and the outflow eigenspaces of the problem.

As before, in the *inflow* eigenspace, a piecewise-constant interpolation is implemented, whereas in the *outflow* eigenspace, an extrapolation from the interior of the domain is utilized to construct a piecewise-linear interpolant.

Moreover, following the general philosophy of the central-schemes, there is no need to work directly in the characteristic inflow/outflow variables – only to identify the corresponding eigenspaces.

3.3 Extensions to the Two-Dimensional Setup

Here, we extend the one-dimensional boundary treatment of §3.1, to the two-dimensional setup. This extension is done dimension by dimension; in each direction we apply the one-dimensional arguments. Following §3.1, we reconstruct in *inflow* boundary cells a constant interpolant from the prescribed boundary data. In *outflow* boundary cells, however, we extrapolate the required quantities at the boundary cells from the interior of the domain.

Again, we deal here only with the first phase of the staggering. We only focus on the left boundary and on the upper-left corner. Analogous treatments hold for the other three boundaries and corners of the stencil. In this two-dimensional case, we approximate solutions to equation (2.6), augmented with boundary conditions at the inflow boundaries. We demonstrate our arguments in the case of the left-boundary (see Figure 4).

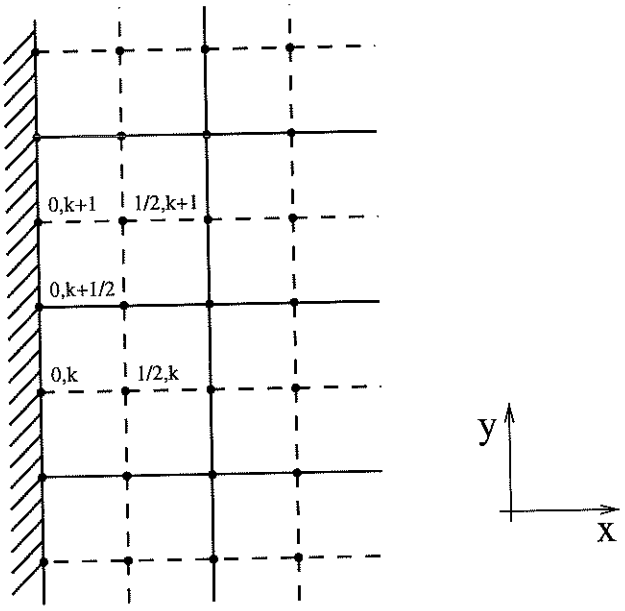

Figure 4: Two dimensions - left boundary

As before, we distinguish between *inflow* ($f'(w^n_{1/2,k}) > 0$), and *outflow* ($f'(w^n_{1/2,k}) < 0$), boundary cells.

In *inflow* boundary cells, we reconstruct a constant interpolant from the prescribed point-values at these boundaries,

$$p_{1/2,k}(x,y,t^n) \equiv w^n_{0,k}, \qquad w'_{1/2,k} = 0. \tag{3.7}$$

This reconstruction is then used to build the approximate solution at time t^{n+1} in the interior cells. At the next-time step, t^{n+1}, the cell-averages at these boundary cells are defined according to the prescribed point-values as

$$\bar{w}^{n+1}_{1/4,k+1/2} := w^{n+1}_{0,k+1/2}.$$

We now turn to the *outflow* boundary cells. Here, we extrapolate the data from the interior of the domain, up to the boundary. First, we determine the discrete slope in the x-direction, $w'_{1/2,k}$. This slope is then used to extrapolate the cell-average up to the boundary,

$$w^n_{0,k} = w^n_{1/2,k} - \frac{\Delta x}{2} w'_{1/2,k},$$

which is then used to predict the mid-value, $w^{n+1/2}_{0,k} = w^n_{0,k} - \frac{\lambda}{2} f'_{0,k} - \frac{\mu}{2} g'_{0,k}$. Here

$$f'_{0,k} = A(w^n_{0,k}) w'_{1/2,k}, \qquad g'_{0,k} = B(w^n_{0,k}) w'_{1/2,k}.$$

The discrete slope in the y-direction, $w'_{0,k}$, is computed in that boundary cell in an analogous way to the interior computation. In summary, the staggered average at time t^{n+1} is given by

$$\bar{w}^{n+1}_{1/4,k+1/2} = \frac{\bar{w}^n_{1/2,k} + \bar{w}^n_{1/2,k+1}}{2} + \frac{1}{8}(-w'_{1/2,k} - w'_{1/2,k+1} + w'_{1/2,k} - w'_{1/2,k+1}) -$$

$$- \frac{\lambda}{2}(f(w^n_{1/2,k+1}) + f(w^n_{1/2,k}) - f(w^n_{0,k+1}) - f(w^n_{0,k})) -$$
$$- \mu(g(w^n_{1/2,k+1}) + g(w^n_{0,k+1}) - g(w^n_{1/2,k}) - g(w^n_{0,k+1})). \tag{3.8}$$

This concludes the boundary treatment of the left boundary. Similar expressions hold for the other three boundaries.

We now turn to the corners and as a prototype, consider the upper-left corner (see Figure 5). In the corner we repeat the previous boundary treatment with one simple modification. The main difference regarding the boundary scheme in the corner is based on the number of different possible inflow/outflow configurations in that corner.

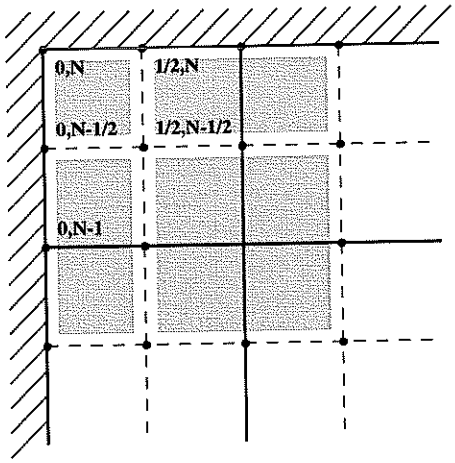

Figure 5: Upper-left corner

In order to avoid spurious oscillations, we reconstruct a constant interpolant whenever *at least* one of the two directions (x or y) is an *inflow* boundary. This is the natural procedure if the flow in both directions is inflow. In this case, the prescribed point-values at the corner should be identical from both directions, a consistency which must already hold in the differential level. In a mixed corner with only one inflow direction, we still employ a constant reconstruction, which prevents data propagation from that corner in the outflow direction; In such case, data can leave the region only through the neighboring boundary cells (see Figure 6). A linear interpolant is reconstructed only if the flow is outflow in both directions.

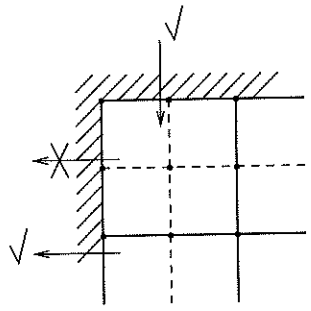

Figure 6: A mixed inflow - outflow corner

Computationally, the most complicated case is when the flow in that upper-left corner is outflow in both directions. In this case, the staggered average at time t^{n+1}, $\bar{w}^{n+1}_{1/4,N-1/4}$, is computed according to

$$\begin{cases} w'_{1/2,N-1/2} = \cdots & \text{Limited slopes} \\ w'_{1/2,N-1/2} = \cdots \end{cases}$$

$$\begin{cases} w^n_{0,N-1/2} = w^n_{1/2,N-1/2} - \frac{\Delta x}{2} w'_{1/2,N-1/2} \\ w^{n+1/2}_{0,N-1/2} = w^n_{0,N-1/2} - \frac{\lambda}{2} f'_{0,N-1/2} - \frac{\mu}{2} g\backslash_{0,N-1/2} \end{cases} \quad \text{Predictor (west)}$$

$$\begin{cases} w^n_{1/2,N} = w^n_{1/2,N-1/2} + \frac{\Delta y}{2} w\backslash_{1/2,N-1/2} \\ w^{n+1/2}_{1/2,N} = w^n_{1/2,N} - \frac{\lambda}{2} f'_{1/2,N} - \frac{\mu}{2} g\backslash_{1/2,N} \end{cases} \quad \text{Predictor (north)}$$

$$\begin{cases} w^n_{0,N} = w^n_{1/2,N-1/2} - \frac{\Delta x}{2} w'_{1/2,N-1/2} + \frac{\Delta y}{2} w\backslash_{1/2,N-1/2} \\ w^{n+1/2}_{0,N} = w^n_{0,N} - \frac{\lambda}{2} f'_{0,N} - \frac{\mu}{2} g\backslash_{0,N} \end{cases} \quad \text{Predictor (north-west)}$$

The cell-average in the north-west edge of Figure 5 in time t^{n+1}, is given in this outflow-outflow case by the *corrector step*

$$\begin{aligned} \bar{w}^{n+1}_{1/4,N-1/4} \;=\; & \bar{w}^n_{1/2,N-1/2} + \frac{-w'_{1/2,N-1/2} + w\backslash_{1/2,N-1/2}}{4} - \\ & -\lambda(f(w^n_{1/2,N}) + f(w^n_{1/2,N-1/2}) - f(w^n_{0,N}) - f(w^n_{0,N-1/2})) - \\ & -\mu(g(w^n_{1/2,N}) + g(w^n_{0,N}) - g(w^n_{1/2,N-1/2}) - g(w_{0,N-1/2})^n). \end{aligned} \tag{3.9}$$

When one of the boundaries is inflow, we have $w'_{1/2,N-1/2} = w\backslash_{1/2,N-1/2} = 0$, and $\bar{w}^{n+1}_{1/4,N-1/4} = w^{n+1}_{0,N}$ (– the prescribed point-values at the corner).

4 Examples of Non-Linear Initial-Boundary Value Problems

Example 1 - 1D Burgers Equation

Our first example approximates the solution of the one-dimensional Burgers Equation,

$$u(x,t)_t + \left(\frac{u^2(x,t)}{2}\right)_x = 0, \quad -1 \le x \le 1,\ 0 <= t, \tag{4.1}$$

subject to the initial conditions, $u(t=0,x) = u_0(x) = 0.2 - \sin\left(\frac{\pi x}{2}\right)$, and to the inflow boundary conditions, $u(-1) = u_0(-1)$, $u(1) = u_0(1)$. In time, the initial condition sharpens, until a discontinuity (shock) is created. This shock moves towards the right boundary, and disappears after 'hitting' it.

Figure 7 shows the evolution of the numerical solution to equation (4.1) in time. The plotted values are the cell-averages. One can clearly see the formation of the shock after a finite time, and the movement of the shock towards the right boundary. Note that no spurious oscillations are created at those inflow boundaries.

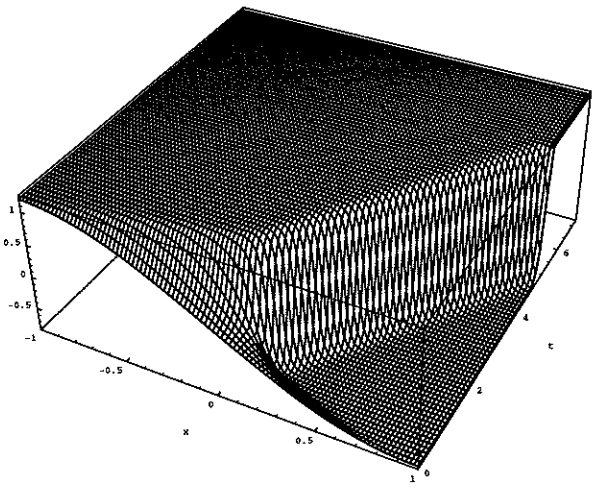

Figure 7: one dimensional Burgers equation (N=101)

Example 2 - 2D Burgers Equation

In this example we approximate a solution to the two-dimensional Burgers equation

$$u_t + uu_x + uu_y = 0, \tag{4.2}$$

subject to the initial conditions,

$$u_0(x,y) = \begin{cases} 0.5 & -1 \le x < 0, -1 \le y < 0 \\ 0 & 0 \le x \le 1, -1 \le y < 0 \\ -1 & 0 \le x \le 1, 0 \le y \le 1 \\ -0.2 & -1 \le x < 0, 0 \le y \le 1. \end{cases}$$

and augmented with boundary conditions at the inflow boundaries which are equal to the initial values at these same boundaries. Figures 8-10 show the evolution of the solution to (4.2) in time for mesh sizes $41 * 41$ and $81 * 81$ as calculated by the algorithm of §3. Again, we note that there are no spurious oscillations at the boundaries, oscillations that are inherent with a naive treatment of inflow boundaries.

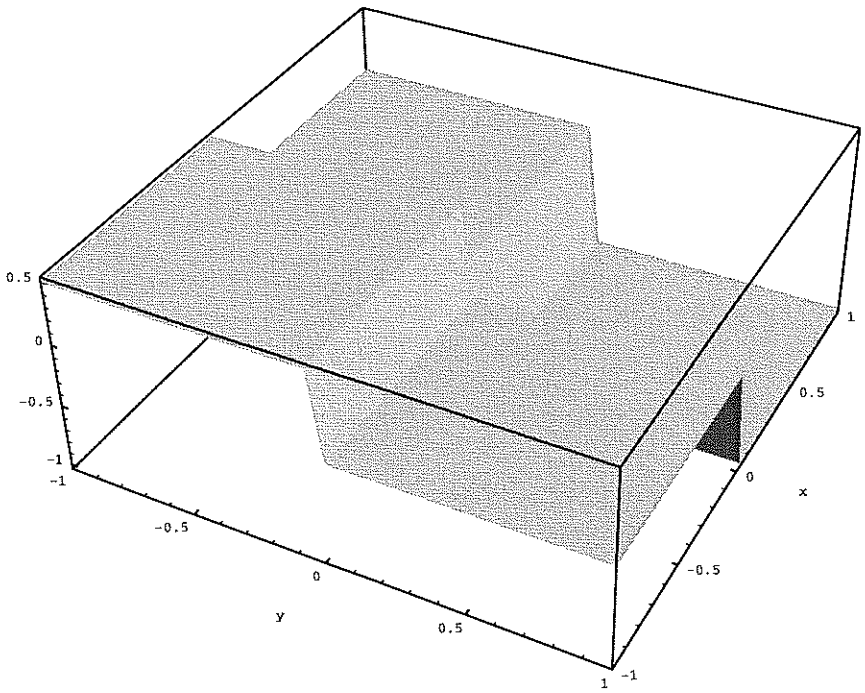

Figure 8: The 2D IBVP Burgers equation, T=0

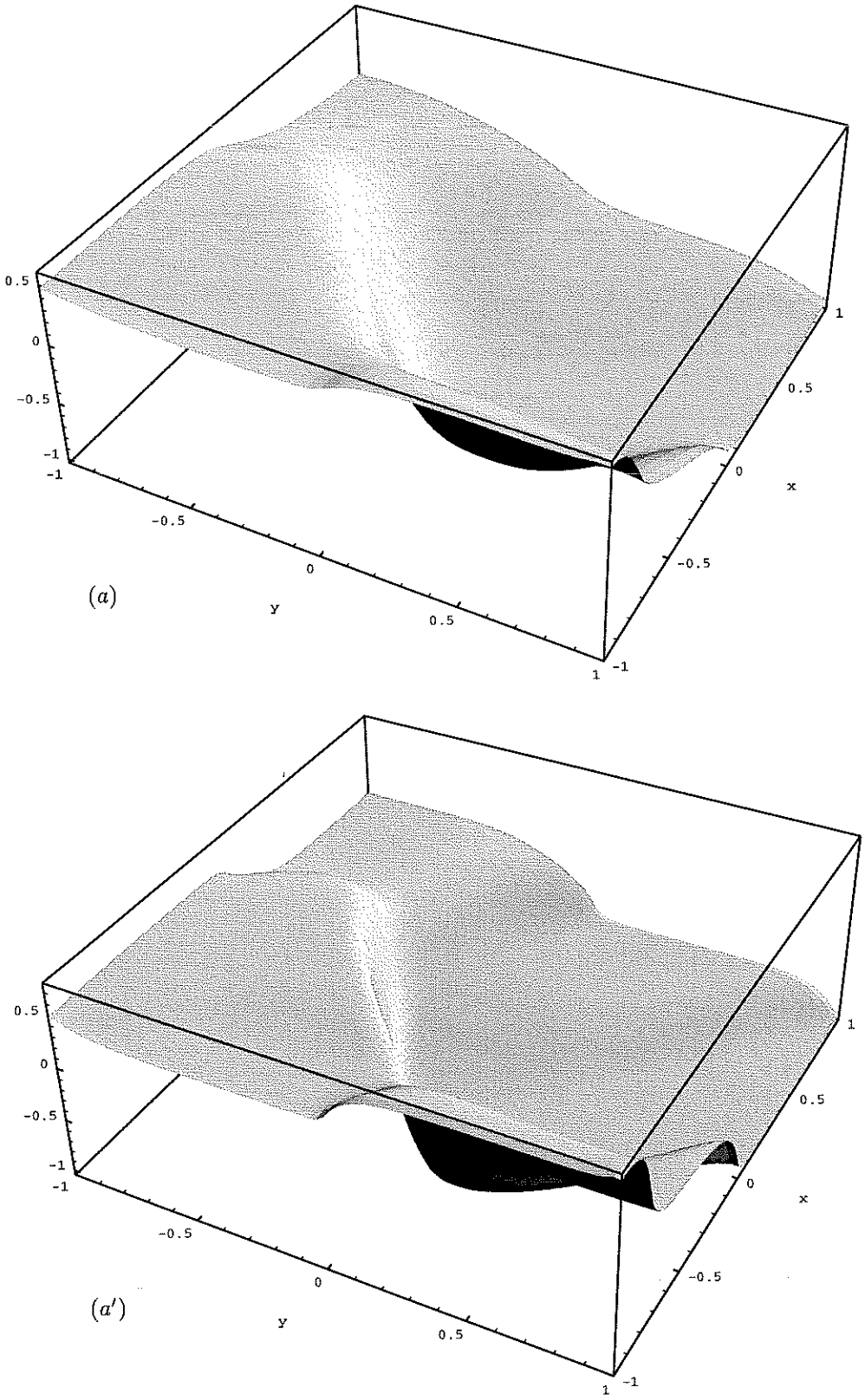

Figure 9: The 2D IBVP Burgers equation: T=1. (a) N=41, (a') N=81

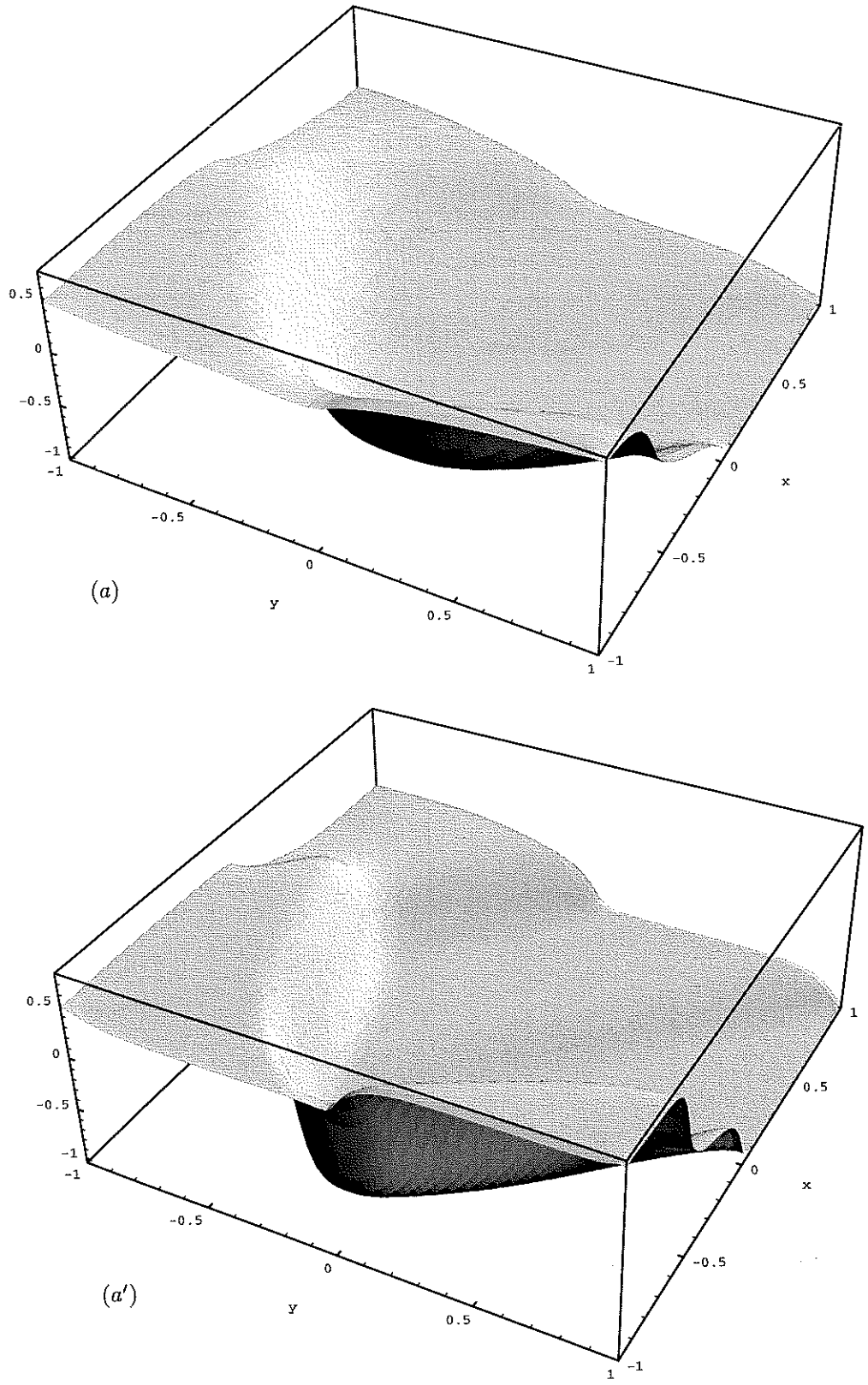

Figure 10: The 2D IBVP Burgers equation: T=2. (a) N=41, (a') N=81

References

[1] Arminjon P., Stanescu D., Viallon M.-C., *A Two-Dimensional Finite Volume Extension of the Lax-Friedrichs and Nessyahu-Tadmor Schemes for Compressible Flow*, (1995), preprint.

[2] Arminjon P., Viallon M.-C., *Généralisation du Schéma de Nessyahu-Tadmor pour Une Équation Hyperbolique à Deux Dimensions D'espace*, C.R. Acad. Sci. Paris, **t. 320** , série I. (1995), pp. 85-88.

[3] Bereux F., Sainsaulieu L., *A Roe-type Riemann Solver for Hyperbolic Systems with Relaxation Based on Time-Dependent Wave Decomposition*, Numer. Math,. **77**, (1997), pp. 143-185.

[4] Friedrichs K. O., Lax P. D., *Systems of Conservation Equations with a Convex Extension*, Proc. Nat. Acad. Sci., **68**, (1971), pp.1686-1688.

[5] Godlewski E., Raviart P.-A., *Hyperbolic Systems of Conservation Laws*, Mathematics & Applications, Ellipses, Paris, 1991.

[6] Harten A., *High Resolution Schemes for Hyperbolic Conservation Laws*, JCP, **49**, (1983), pp.357-393.

[7] Huynh H. T., *A Piecewise-parabolic Dual-mesh Method for the Euler Equations* (1995), preprint.

[8] Jiang G.-S., Tadmor E., *Nonoscillatory Central Schemes for Multidimensional Hyperbolic Conservation Laws*, SIAM J. Scie. Comp., to appear.

[9] Jin S., private communication.

[10] van Leer B., *Towards the Ultimate Conservative Difference Scheme, V. A Second-Order Sequel to Godunov's Method*, JCP, **32**, (1979), pp.101-136.

[11] LeVeque R. J., *Numerical Methods for Conservation Laws*, Lectures in Mathematics, Birkhauser Verlag, Basel, 1992.

[12] Levy D., *Third-order 2D Central Schemes for Hyperbolic Conservation Laws*, in preparation.

[13] Levy D., Tadmor E., *Non-oscillatory Central Schemes for the Incompressible 2-D Euler Equations*, Math. Res. Let., **4**, (1997), pp.321-340.

[14] Liu X.-D., Osher S., *Nonoscillatory High Order Accurate Self-Similar Maximum Principle Satisfying Shock Capturing Schemes I*, SINUM, **33**, no. 2 (1996), pp.760-779.

[15] Liu X.-D., Tadmor E., *Third Order Nonoscillatory Central Scheme for Hyperbolic Conservation Laws*, Numer. Math., to appear.

[16] Nessyahu H., Tadmor E., *Non-oscillatory Central Differencing for Hyperbolic Conservation Laws*, JCP, **87**, no. 2 (1990), pp.408-463.

[17] Osher S., Tadmor E., *On the Convergence of Difference Approximations to Scalar Conservation Laws*, Math. Comp., **50**, no. 181 (1988), pp.19-51.

[18] Roe P. L., *Approximate Riemann Solvers, Parameter Vectors, and Difference Schemes*, JCP, **43**, (1981), pp.357-372.

[19] Runborg O., *Multiphase Computations in Geometrical Optics*, UCLA CAM report no. 96-52 (1996).

[20] Sanders R., *A Third-order Accurate Variation Nonexpansive Difference Scheme for Single Conservation Laws*, Math. Comp., **41** (1988), pp.535-558.

[21] Sanders R., Weiser A., *A High Resolution Staggered Mesh Approach for Nonlinear Hyperbolic Systems of Conservation Laws*, JCP, **1010** (1992), pp.314-329.

[22] Sweby P. K., *High Resolution Schemes Using Flux Limiters for Hyperbolic Conservation Laws*, SINUM, **21**, no. 5 (1984), pp.995-1011.

[23] Tadmor E., Wu C.C., *Central Scheme for the Multidimensional MHD Equations*, in preparation.